Electrochemical lithiation of Pb_3O_4

C. Barriga*, S. Maffi and **L. Peraldo Bicelli****

Department of Applied Physical Chemistry of the Milan Polytechnic, Research Centre on Electrode Processes of the CNR, Piazza Leonardo da Vinci 32, 20133 Milan (Italy)

C. Malitesta

Analytical Chemistry Laboratory, Department of Chemistry, University of Bari, 4 Trav. Re David 200, 70126 Bari (Italy)

Abstract

Pb_3O_4 has been investigated as a cathode material for voltage compatible, nonaqueous lithium cells and its good performance has been demonstrated. The mechanism of the process has been elucidated by undertaking X-ray and XPS analyses of the discharge products at significant points of the discharge curve. Pb(II) was unambiguously recognized by the latter technique, thus evidencing a two-step reduction mechanism *en route* to Pb(0) during lithiation.

Introduction

Pb_3O_4 is one of the lead oxides that has already been investigated by Gabano and coworkers [1, 2] as cathode materials for voltage compatible, nonaqueous lithium cells, and it was found to be the most suitable material for practical applications [2], as more recently confirmed by Wiesener and coworkers [3]. In fact, the discharge curves of the Li/Pb_3O_4 cells are characterized by a very extended plateau having the highest voltage value (1.5 V) of the other Li/lead oxide cells [1]. Although according to thermodynamics Pb_3O_4 is expected to present two distinct plateaux, the first corresponding to the initial reduction to PbO and the second to PbO reduction to Pb [4], only one plateau was observed [1–3, 5]. By contrast, two distinct plateaux were found for PbO_2 [3, 5–7] and XPS analysis was able to relate them to the two above-mentioned processes [8]. Moreover, taking the kinetic and solid-state aspects of the same processes into account, it was also possible to explain why the first plateau is much shorter than the second. In fact, while PbO_2 reduction proceeds, a layer of PbO and Li_2O builds-up, decreasing

---

*On leave from Departamento de Quimica Inorganica e Ingenieria Quimica, Facultad de Ciencias, Universidad de Cordoba, Spain.
**Author to whom correspondence should be addressed.

the surface area available for the reaction. When the system can no longer sustain the fixed current, the voltage control switches to PbO reduction to Pb, i.e., to the second plateau.

Although, as previously stated, only one plateau was noted during Pb_3O_4 discharge in lithium cells, a recently performed comprehensive analysis [3] has shown the reduction process of Pb_3O_4 to Pb to proceed via the two, already mentioned, partial steps which run simultaneously. While, at the beginning of the discharge, the reduction of Pb^{4+} to Pb^{2+} dominates, it is the reduction of Pb^{2+} to Pb at the phase interface which determines the voltage plateau. At the same time, Pb^{4+} is reduced in the bulk of the Pb_3O_4 particles.

As part of a research project on lead oxides which has already considered PbO [6] and PbO_2 [6, 8], the discharge behaviour of Pb_3O_4 in lithium cells was examined, aiming on the one hand to investigate in depth the electrochemical aspects in connection with the appearance of typical plateaux, and, on the other hand, to investigate the reduction mechanism by carrying out X-ray and XPS analyses of the discharge products at significant points on the discharge curve.

Experimental

Pb_3O_4, minium, having a tetragonal unit cell, was a 99% purity Aldrich-Chemie product. Its structure was confirmed by X-ray diffraction. The same technique was also employed to examine structural changes occurring on the cathode material after lithiation at several depths of discharge. X-ray diffraction was carried out with a Siemens D500 diffractometer, using Cu $K\alpha$ radiation monochromated by a graphite crystal. The X-ray line profiles were used in intensity measurements and precision determinations of lattice parameters and recorded by step-scan with step sizes of $0.02°$ 2θ. The size of coherently diffracting domains and the content of microstrains were estimated by profile fitting to Pearson-VII function [9]. A highly crystalline sample of lead nitrate provided the instrumental profiles.

After discharging, cells were disassembled and cathodes transferred to the XPS apparatus under as clean as possible conditions, avoiding contact with air. XP spectra were collected by a Leybold LHS 10 spectrometer, equipped with unmonochromatized Mg $K\alpha$ and Al $K\alpha$ sources (generally operated at 280 W) and controlled by an Apple II microcomputer [8]. Samples were mounted on a conducting adhesive tape. Widescan spectra (CRR mode, retarding ratio 3, Mg $K\alpha$, Al $K\alpha$ radiations) and Pb4f, C1s, O1s region spectra (CAE mode, pass energy 50 eV, Mg $K\alpha$ radiation) were recorded. Full details on data acquisition and the processing system are reported elsewhere [8].

Thermogravimetric (TGA) and differential scanning calorimetry (DSC) analyses were performed at a heating rate of 10 °C min^{-1} in dry, and oxygen-free nitrogen.

Electrochemical investigations were carried out in a dry box under argon atmosphere using standard equipment with two- and three-electrode test cells.

The cathode mixture consisted of 90 wt.% active material and 10 wt.% Teflon organic binder, and the pellets were prepared by pressing 50–100 mg of the powder, at 350 MPa, on an inert metallic copper substrate (99% reduced copper, Carlo Erba). The cathode pellet (12 mm dia.) was separated from the lithium disc anode (greater than 99% lithium, Alfa Ventron) by porous glass-paper-discs soaked with the electrolyte. The latter was 1 M $LiClO_4$ either in propylene carbonate (PC) or in a 1:1 mixture of PC and 1,2-dimethoxyethane (DME), the latter being the electrolyte usually employed. Preliminary solubility tests proved Pb_3O_4 to be insoluble in the electrolytes used. Computer-assisted galvanostatic discharge measurements were performed at several current densities and step polarization tests were performed at increasing, and subsequently decreasing, current densities (sequence of galvanostatic pulses lasting 30 s, the circuit being opened for 30 s after each pulse). All experiments were carried out at room temperature. For more details, please see ref. 10.

Results and discussion

Material characterization

Figure 1 depicts the TGA and DSC curves of Pb_3O_4, which are strongly correlated, particularly at the highest temperatures. Decomposition of Pb_3O_4 to PbO starts at low temperatures and seems to occur in two steps. While the former involves a very small weight decrease, formally from Pb_3O_4 to $Pb_3O_{3.83}$, the second step (around 550 °C) implies the complete decomposition of the material to yellow PbO, as also shown from the change in the colour of the residual material. The total weight loss (2.55 wt.%) is somewhat higher than theoretically calculated for the above reaction (2.34 wt.%) and this difference cannot be ascribed to the presence of water as no weight losses occurred up to 150 °C. Perhaps our specimens were oxidized and contained small quantities of PbO_2, not recognized by X-ray analysis.

With regard to thermal measurements, the maximum endothermal effect occurs at about 565 °C and the absorbed heat (118.1 J g^{-1}) is larger than that calculated from thermodynamic data under standard conditions (about 97 J g^{-1}) [11].

The disagreement between experimental and theoretical values is much greater here than for TGA results. It may partly be due to uncertainties in thermodynamic data, surely less precise than molecular weights. Moreover, they refer to standard conditions. In addition, calorimetric determinations are expected to be less accurate than thermogravimetric ones. A similar trend (higher experimental than thermodynamic values) was also observed previously during PbO_2 thermal reduction to PbO [6].

According to literature data [12a], Pb_3O_4 loses oxygen and converts to PbO on heating in air at temperatures higher than 550 °C. Moreover, PbO
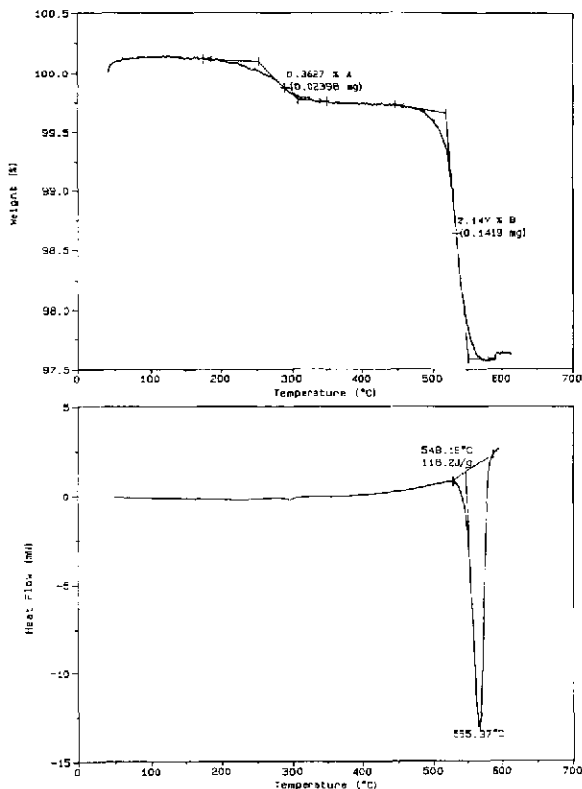
Fig. 1. Thermogravimetric analysis curve (TGA) and differential scanning calorimetry spectrum (DSC) of Pb_3O_4.

gives rise to an endothermic transition from the red (tetragonal) to the yellow (orthorhombic) phase at 489 °C [12b] and, in fact, this is the phase observed at the end of our heating process.

SEM analysis of the pellet (Fig. 2) evidences the material inhomogeneity. In fact, macrodispersion (dark spots) as well as microdispersion of PTFE is clearly noticeable on the cathode surface. The dark spots were recognized by microprobe analysis to contain carbon and fluorine only, whereas lead and oxygen were the main components of the other regions. Such morphology is a consequence of Pb_3O_4 being a rather fine powder (the BET surface area was around 9 m^2 g^{-1}) while the Teflon powder was much coarser and practically impossible to grind. On the other hand, it was not possible to avoid PTFE addition to Pb_3O_4 since the binder was necessary to ensure the mechanical stability of the cathode.

Electrochemical results

Electrochemical lithiation was carried out in cells of the type

(−) Li/electrolyte/cathode pellet (+)
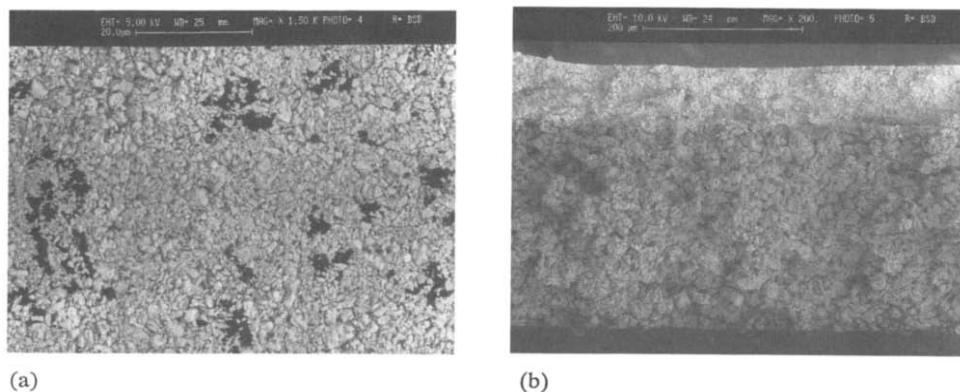
Fig. 2. SEM micrographs of the surface (a) and cross section (b) of a 90 wt.% Pb_3O_4 + 10 wt.% PTFE pellet.
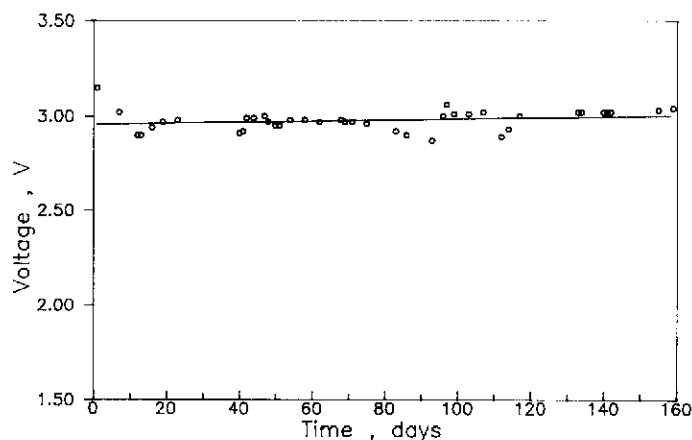
Fig. 3. Open circuit voltage as a function of time of a fresh Li/1 M $LiClO_4$–PC + DME/90 wt.% Pb_3O_4 + 10 wt.% PTFE cell.

whose open circuit voltages were preliminarily checked in long-term experiments. An example is depicted in Fig. 3. The initial value of the open circuit voltage is greater than 3 V, as was also found for several cells employed in other types of experiments. It oscillates slightly, reaching a nearly constant value after several months. At the end of the test, lasting 160 days, the cell presented the usual discharge characteristics, so that no capacity losses were observed.

In order to examine how the values of closed circuit voltages are influenced by the discharge rate and how many electrons are involved in the cell reaction, discharge tests at different current densities were performed. Typical curves are shown in Fig. 4 where the abscissa refers to the circulated number of moles of electrons for each mole of the compound and, in the case where no parasitic reactions took place (e.g., electrolyte decomposition), to lithium
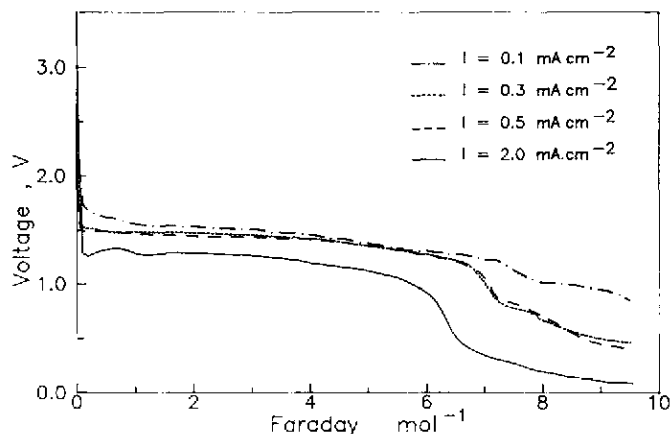
Fig. 4. Discharge characteristics of Li/1 M LiClO$_4$–PC+DME/90 wt.% Pb$_3$O$_4$+10 wt.% PTFE cells at different current densities.

equivalents discharged, again per mole of the oxide. For sake of completeness, almost the whole discharge range, i.e., down to very low cell voltages, was reported in this and in the other relevant figures.

The curves in Fig. 4 are characterized by a quasi-plateau whose length and voltage usually decrease when increasing the rate of the process. However, some overlapping of the experimental curves is noted in the case where the tests slightly differ in current density, an indication of the scarce reproducibility of the measurements.

The discharge plateau, typical of a multiphase system, is connected to the Pb$_3$O$_4$ reduction process to lead, as also evidenced by X-ray measurements (see below). The maximum length of the plateau is about 7.2 lithium equivalents per Pb$_3$O$_4$ mole, i.e., close to the theoretical value (8 Faraday per mole) for a fully discharged pellet, while the maximum voltage value is around 1.6 V. Owing to ohmic voltage drops (no electronically conductive agents were added to the active compound) and kinetics contributions, the latter value is much lower than the thermodynamic value for Pb$_3$O$_4$ reduction to PbO and to Pb, and for PbO reduction to Pb: 2.73, 2.13, and 1.94 V versus Li/ Li$^+$, respectively, under standard conditions [4]. No information on the reduction mechanism may therefore be deduced from these data. The mechanism will be discussed later, mainly considering the first part of the discharge curves not examined here.

All the experiments were carried out in the PC+DME electrolyte which combines the high conductivity of PC with the high fluidity of DME. Indeed, the PC+DME electrolyte is expected to give better results than the customary PC electrolyte, as has been verified experimentally [13]. However, this seems not to occur in the case of Pb$_3$O$_4$, as shown in Fig. 5, where the differences in the material discharge properties in the two electrolytes are of the order of the measurement reproducibility. A greater stability to electrochemical
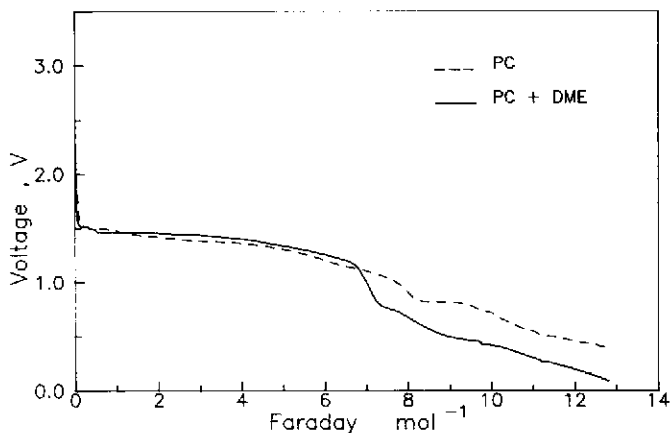
Fig. 5. Discharge characteristics of the Li/1 M LiClO$_4$–PC+DME/90 wt.% Pb$_3$O$_4$+10 wt.% PTFE cell (——), and of the Li/1 M LiClO$_4$–PC/90 wt.% Pb$_3$O$_4$+10 wt.% PTFE cell (– – –) at 0.3 mA cm^{-2}.

decomposition is presented by PC in comparison to PC+DME electrolyte, however.

From the curves reported in Fig. 4, we determined the Li/Pb$_3$O$_4$ cell properties at the various current densities summarized in Table 1. The cut-off voltage was 1 V. The specific and volumetric energies were based on the weight and volume of the active material only, and were estimated by the related capacities and average cell discharge voltages.

Table 1 evidences the good performance of the system examined; Li/Pb$_3$O$_4$ cells show mean discharge voltages decidedly higher than Li/PbO$_2$ cells (e.g., 1.38 instead of 1.27 [6] V at 0.5 mA cm^{-2}) but lower specific capacities and energies (0.27 instead of 0.37 [6] A h g^{-1} and 0.38 instead of 0.47 [6] W h g^{-1}, respectively, at the same current density). According to theoretical calculations [14], the specific energy of Pb$_3$O$_4$ is very high (0.435 W h g^{-1}).

As already observed by Wiesener and coworkers [3], reduction efficiencies higher than 100% can be noted at the lowest current densities (Fig. 4 and Table 1). Since the cut-off voltage considered is 1 V, solvent decomposition is not expected to occur to any measurable extent. More probably, electrochemical alloying of lithium with lead takes place, as found by Dey [15] in Li/1 M LiClO$_4$–PC/Pb cells. Indeed, lithium is known to form several intermetallic compounds with lead (LiPb; Li$_5$Pb$_2$; Li$_3$Pb; Li$_{10}$Pb$_3$; Li$_7$Pb$_2$; Li$_4$Pb [16]), and Dey found a composition very close to Li$_{10}$Pb$_3$ after 450 h discharge of the cell on a 1 kΩ external load. However, no evidence of the alloys was found in X-ray and XPS data relative to our discharged samples.

For a better insight into the discharge kinetics, particularly in view of practical applications, step polarization tests in three-electrode cells were performed. From the results reported in Fig. 6, it turns out that cathode potentials (after a 30 s pulse) higher than 1 V versus Li/Li$^+$ are obtained

TABLE 1

Performance of Pb_3O_4 in 1 M $LiClO_4$–PC+DME lithium cells at several current densities (cut-off voltage: 1 V)

Current density (mA cm⁻²)	Average voltage (V)	Depth of discharge (Li eq mol⁻¹)	Specific and volumetric capacity[a]		Specific and volumetric energy[a]	
			A h g⁻¹	A h cm⁻³ [b]	W h g⁻¹	W h cm⁻³ [b]
0.1	1.40	8.41	0.329	2.994	0.460	4.186
0.3	1.38	7.00	0.274	2.493	0.377	3.431
0.5	1.38	7.07	0.276	2.512	0.381	3.467
2	1.25	5.71	0.227	2.066	0.283	2.575

[a]Based on active material.
[b]Assuming a density of 9.1 g cm⁻³ [12(c)].
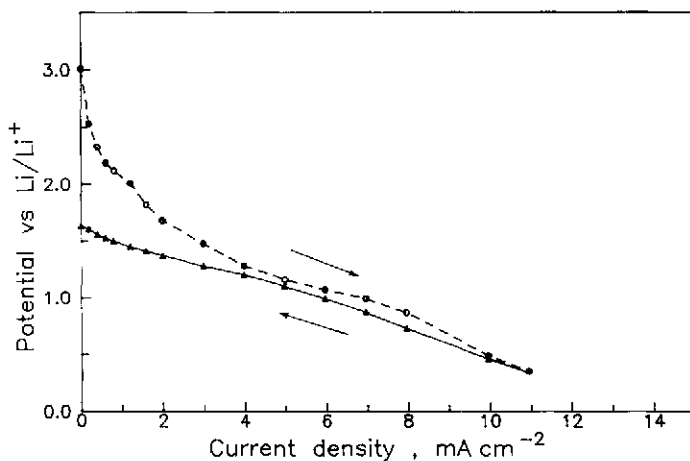
Fig. 6. Dependence of the potential after a 30 s pulse as a function of Li/Li^+ on increasing (○) and decreasing (△) current density values of a 90 wt.% Pb_3O_4 + 10 wt.% PTFE cathode in 1 M $LiClO_4$–PC + DME from galvanostatic step polarization tests.

up to current densities as high as 7 mA cm^{-2}. This confirms the satisfactory behaviour of the material.

In spite of the small quantities of lithium discharged (a total of about 0.3 equivalents per mole, assuming that no significant electrolyte decomposition took place) the values of the potential at the end of the experiment were decidedly smaller than the initial ones. This could be a consequence of permanent modifications in the electrode composition mainly occurring at the pellet interface.

X-ray results

In order to study the different phases present after progressive lithiation, X-ray diffraction analysis was carried out. Figure 7 depicts the X-ray diffraction patterns of the Pb_3O_4 powder (a) and pellet (b), and of the Pb_3O_4-containing pellets after progressive lithiation (c)–(i). Up to the discharge of 0.1 lithium equivalents per mole of the compound, the pattern remains practically unchanged. At 1 lithium equivalent per mole, the lines due to Pb_3O_4 still dominate but reflections due to Pb are also present. This indicates that full reduction of the compound is already accomplished but probably not on the whole sample. Indeed, owing to the different colours of the Pb_3O_4 pellet before, and after, electrochemical lithiation, it was still possible to distinguish a yellowish border, due to the original oxide, from the otherwise dark material at the cathode surface. By increasing the discharged lithium quantities, the lines due to Pb grow in intensity, so that after a deep discharge (6 lithium equivalents per mole) Pb_3O_4 has almost disappeared. With regard to the presence of PbO, there is a lack of evidence of the yellow phase, whereas the red phase cannot, unambiguously, be excluded. Indeed, the line around 28.7° 2θ is sometimes very intense in the pattern of the discharged specimens. It may be assigned to both the red PbO 101 line (28.64° [17]) and the
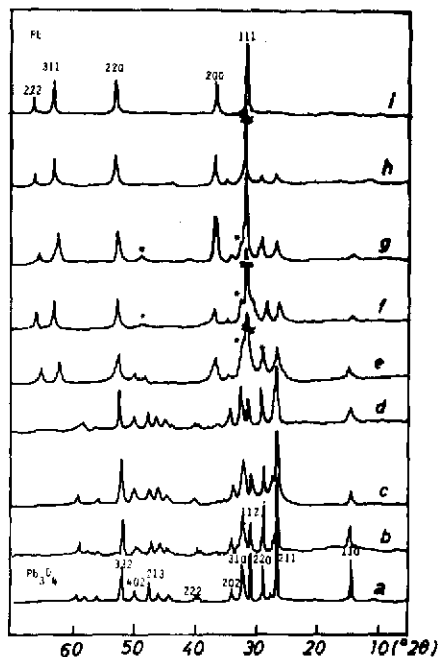
Fig. 7. X-ray diffraction pattern (Cu Kα) of the pure 90 wt.% Pb₃O₄ + 10 wt.% PTFE powder
(a) and pellet (b), and of the same pellet after lithium discharge up to 0.1 (c), 1.0 (d), 2 (e),
3 (f), 4 (g), 5 (h), and 6 (i) Faraday mol⁻¹. (∗) refers to possible lines of red PbO.

Pb_3O_4 220 line (28.68° [18]). However, since in the pattern of our Pb_3O_4 powder and pellet this peak is more intense than is found experimentally in polycrystalline samples [18], preferred orientation effects are also possible. Furthermore, the next two most intense reflections of red PbO are absent.

The structural parameters for the Pb_3O_4 332 and the Pb 311 and 200 reflections are shown in Table 2. The most relevant feature of these results is the higher crystallinity of the nearly unchanged pellet (0.1 lithium equivalents per mole). At the beginning of the discharge, the domain size is relatively large, whereas, when the discharged lithium quantity increases, the reduction of Pb_3O_4 is accompanied by a loss of crystallinity, the crystallite size decreases while the microstrain content remains practically constant. So, lead has formed following a rupture of the Pb_3O_4 crystallites at the beginning of the discharge. On the other hand, the crystallinity of such reduction products is hardly modified with increasing lithium discharge, as can be seen in Table 2.

The unit cell parameters of tetragonal Pb_3O_4 and cubic Pb were obtained by the least-square method. The results are shown in Table 3. It was observed that the unit cell volume of Pb_3O_4 decreases slightly with progressive lithiation. This effect may be due to the formation of other phases. The reduction of Pb_3O_4 to PbO is accompanied by a decrease in the molar volume. This is in line with the thermal reduction of lead oxides which occurs continuously

TABLE 2

Structural parameters for several selected discharged pellets

Li (eq mol^{-1})	Pb$_3$O$_4$ 332 reflections			
	FWHM	m	$\bar{e} \times 10^3$	D (Å)
0.1	0.28	2.4	1.9	1162
1.0	0.33	2.0	2.2	682
2.0	0.32	1.9	2.1	636

	Pb 311 reflections				Pb 200 reflections			
	FWHM	m	$\bar{e} \times 10^3$	D (Å)	FWHM	m	$\bar{e} \times 10^3$	D (Å)
3.0	0.39	2.2	2.0	582	0.31	1.4	1.7	359
4.0	0.44	2.1	2.4	489	0.42	1.2	2.3	204
5.0	0.44	1.7	2.3	442	0.40	1.4	2.8	276

FWHM: Full width at half maximum (°2θ).
m: Exponent of Pearson VII function.
$\bar{e}$: Weighed average microstrain content.
D: Crystallite size.

TABLE 3

Unit cell parameters for Pb$_3$O$_4$ and Pb

Pb$_3$O$_4$ tetragonal ($P4_2/mbc$)			Pb cubic ($Fm3m$)	
Li eq mol^{-1}	a (Å)	c (Å)	Li eq mol^{-1}	a (Å)
0.1	8.81$_0$	6.55$_8$	3.0	4.95$_0$
1.0	8.81$_6$	6.55$_7$	4.0	4.93$_5$
2.0	8.75$_8$	6.54$_7$	5.0	4.94$_7$
			6.0	4.94$_9$

[19]. The final product of the discharge is Pb metal whose XRD lines show little change in their position.

XPS results

In order to show the existence of a second plateau, low-rate experiments were carried out (at current densities lower than 0.1 mA cm^{-2}) and the discharge curves analyzed in more detail, particularly enlarging their initial part up to 0.3 lithium equivalents per mole. A typical example obtained at a current density of 0.05 mA cm^{-2} is shown in Fig. 8. A very short plateau around 2.3 V is seen, followed by a more extended plateau at about 1.85 V. The voltage value of the former plateau allows its exclusion as being due to the direct reduction of Pb$_3$O$_4$ to Pb, since it is higher than the thermodynamic value (2.13 V versus Li/Li$^+$). Low-rate discharge therefore gives evidence of
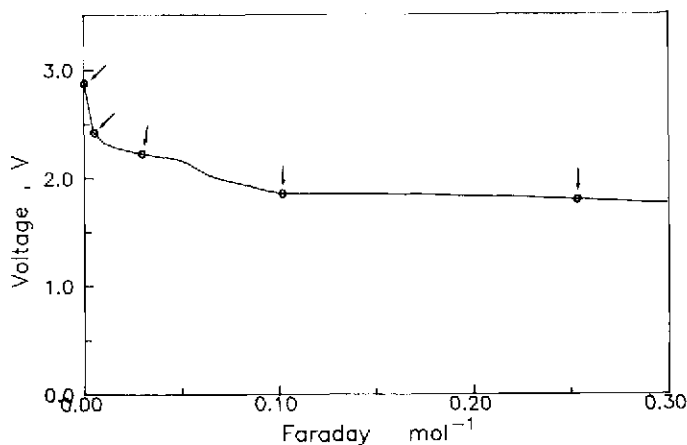
Fig. 8. Low rate (0.05 mA cm^{-2}) discharge characteristics of the Li/1 M LiClO$_4$–PC+DME/ 90 wt.% Pb$_3$O$_4$ + 10 wt.% PTFE cell to give evidence of the main discharge plateaux. Arrows indicate the collocation on the curve of the XPS analysed cathodes (original pellet and after lithium discharge up to 0.01, 0.03, 0.1 and 0.25 Faraday mol^{-1}).
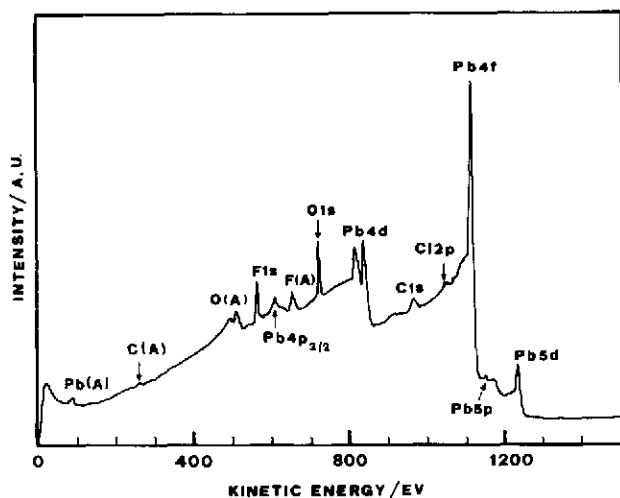
Fig. 9. Widescan spectrum of a Pb$_3$O$_4$ cathode discharged up to 0.1 Faraday mol^{-1}. Radiation source: Mg Kα. Kinetic energy scale uncorrected for charging. The A label marks Auger peaks.

Pb$_3$O$_4$ lithiation taking place via two reduction steps, although the main discharge voltage at constant current density is still determined by the second step. It occurs at the solid–liquid interface, immediately reducing the PbO produced on the external surface area of the crystallites to Pb, in agreement with ref. 3. This could explain the difficulties met with in this paper in evidencing PbO reflections in the X-ray diffraction patterns of the discharged cathodes, and the absence of such peaks noted by Ohzuku et al. [5].

As already shown [8], this limitation can be overcome by XPS. To this end, the original pellet and the pellets discharged up to 0.01, 0.03, 0.1 and

0.25 Faraday mol^{-1} have been analyzed by this technique. Figure 9 shows a typical widescan spectrum recorded on a discharged cathode. The expected elemental composition is revealed, as well as the presence of some electrolyte contamination.

Detailed Pb 4f spectra of most cathodes exhibited symmetric peaks (Fig. 10(a), (b)) with small changes of width, easily correlated with the charging status, as inferred from the change of width of the corresponding C 1s signal. Not all were clearly asymmetric (Fig. 10(c)). 'Symmetric' Pb 4f spectra were fitted by one doublet (splitting 4.9 eV, ratio = 0.75 [8]), while for the 'asymmetric'-shaped signals two doublets of the same width were successfully employed. O 1s spectra were also fitted and an oxide component [8] was always evidenced; often, a carbonate contribution also appeared.

Table 4 reports the results of the above analysis. A comparison with literature data [8] allows only the unequivocal assignment of Pb(II) species in specimens discharged at 0.03, 0.1 and 0.25 Faraday mol^{-1} (in the latter case, the high binding energy component only is referred to) (Table 4). In
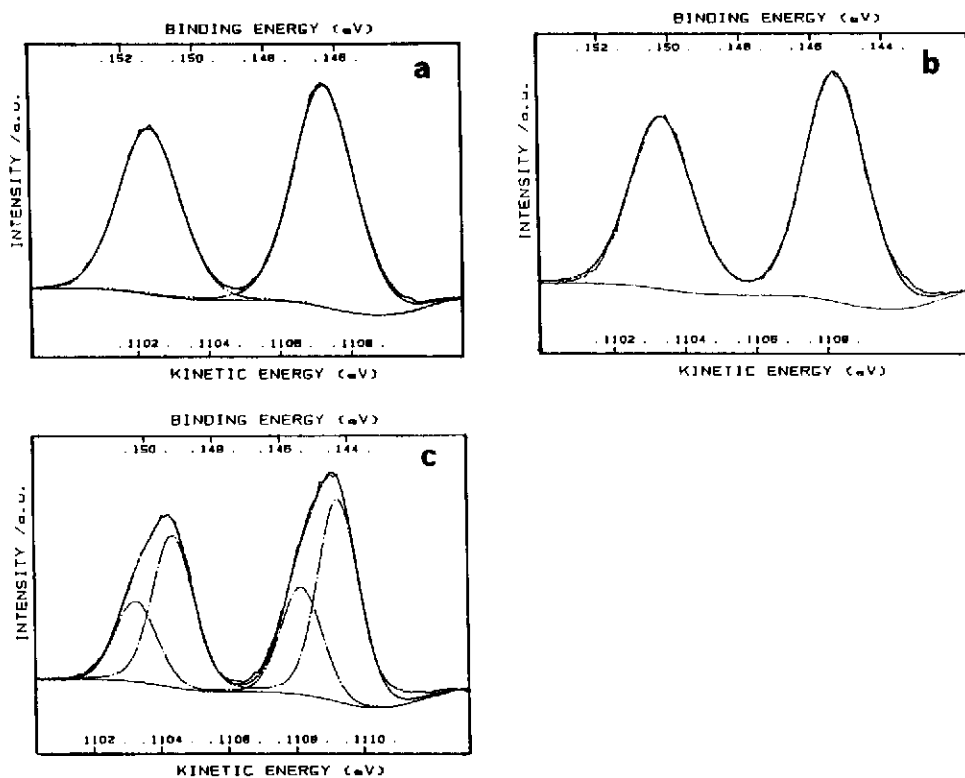
Fig. 10. XP fitted spectra of the Pb 4f region recorded on Pb$_3$O$_4$ cathodes: cathode blank (a), and cathodes discharged up to 0.03 (b), and 0.25 (c) Faraday mol^{-1}. Radiation source: Mg Kα. Energy scales uncorrected for charging.

TABLE 4

Pb $4f_{7/2}$ and O 1s (oxide component) BE[a] obtained by fitting XP spectra recorded on cathodes

Depth of discharge (Li eq mol^{-1})	Pb $4f_{7/2}$ (eV)		O 1s (eV)
Cathode blank		137.9	529.1
0.01		137.8	529.6
0.03		138.4	529.2
0.1		138.5	529.4
0.25	139.2	138.1	529.6

[a]Values are adjusted to Au $4f_{7/2}$ = 84.0 eV, Cu $2p_{3/2}$ = 932.6 eV, and C 1s = 284.8 eV. Reproducibility is ±0.2 eV.

this case, the oxide to lead ratio evaluations [8] were not helpful, as they did not produce unequivocal attributions.

The above findings are the first direct evidence for the presence of Pb(II) species in partially discharged cathodes, and the occurrence of such a species in the high- and low-voltage plateau agrees with thermodynamics and the hypothesised mechanism (see above).

Lead was not recognized in specimens discharged at 0.25 Faraday mol^{-1}, i.e., at the very beginning of the main discharge plateau (Fig. 4). This absence may be explained considering that small Pb particles are highly reactive and that the reaction

$$Pb + Pb_3O_4 = 4PbO$$

is favourite according to thermodynamic calculations [4]. Furthermore, the presence of carbonates in the system may possibly be due to side reactions of basic oxides (PbO, Li_2O) with the solvent [20].

Conclusions

The main results of this paper can be summarized as follows:

(i) Pb_3O_4 starts decomposing at around 200 °C, such decomposition occurring in two steps. The first involves a very small weight decrease (to formally $Pb_3O_{3.83}$) while the second, beginning at around 550 °C, produces the complete decomposition to PbO.

(ii) Up to 7 lithium equivalents per mole can be discharged in Li/Pb_3O_4 cells at a current density of 0.5 mA cm^{-2}. An extended plateau at about 1.4 V is observed in these conditions, whereas an additional plateau at much higher values (e.g., 2.3 V) could be evidenced at very small current densities (e.g., 0.05 mA cm^{-2}).

(iii) X-ray diffraction analysis of the electrochemically lithiated Pb_3O_4 pellets shows that Pb_3O_4 reduction to Pb takes place. The results are confirmed by XPS investigations which, in addition, give direct evidence of the presence

of Pb(II) species in partially discharged cathodes, in agreement with the two-step-mechanism ($Pb_3O_4 \rightarrow PbO \rightarrow Pb$) suggested by Wiesener and co-workers [3].

Acknowledgements

References

1 M. Broussely, Y. Jumel and J. P. Gabano, *Power Sources 7*, Academic Press, London, 1979, p. 637.
2 M. Broussely, Y. Jumel and J. P. Gabano, *J. Power Sources, 5* (1980) 83; M. Broussely and Y. Jumel, in J. P. Gabano (ed.), *Lithium Batteries*, Academic Press, London, 1983, p. 97.
3 G. Ludwig, W. Schneider and K. Wiesener, *J. Power Sources, 21* (1987) 105.
4 L. Peraldo Bicelli, *Mater. Chem. Phys., 25* (1990) 207.
5 T. Ohzuku, T. Shimamoto and T. Hirai, *Electrochim. Acta, 26* (1981) 751.
6 L. Peraldo Bicelli, B. Rivolta, F. Bonino, S. Maffi and C. Malitesta, *J. Power Sources, 18* (1986) 63.
7 T. Kahara, T. Horiba, K. Tamura and M. Fujita, *Proc. Electrochem. Soc., 80-4* (1980) 300.
8 C. Malitesta, L. Sabbatini, P. G. Zambonin, L. Peraldo Bicelli and S. Maffi, *J. Chem. Soc., Faraday Trans. I, 85* (1989) 1685.
9 Th. H. De Keijser, E. Mittemeijer and H. C. F. Rozendaal, *J. Appl. Crystallogr., 16* (1983) 309.
10 M. Boccoli, F. Bonino, M. Lazzari and B. Rivolta, *Solid State Ionics, 7* (1982) 65.
11 D. D. Wagman, W. H. Evans, V. B. Parker, H. Schumm, I. Halow, S. M. Bailey, K. L. Churney and R. L. Nuttall, *J. Phys. Chem. Ref. Data, 11* (Suppl. 2) (1982) 2–119.
12 G. V. Samsonov, *The Oxide Handbook*, IFI Plenum, New York, 1973; (a) p. 221; (b) p. 161; (c) p. 35.
13 G. Pistoia, M. Pasquali, M. Tocci, V. Manev and R. V. Moshtev, *J. Power Sources, 15* (1985) 13.
14 J. Desilvestro and O. Haas, *J. Electrochem. Soc., 137* (1990) 5c.
15 A. N. Dey, *J. Electrochem. Soc., 118* (1971) 1547.
16 W. B. Pearson, *A Handbook of Lattice Spacings and Structures of Metals and Alloys*, Pergamon, London, 1958, p. 717.
17 *ASTM Card, 5-0561*, 1974.
18 *ASTM Card, 8-19*, 1967.
19 P. Boher, P. Garnier, J. R. Gavarri and D. Weigel, *J. Solid State Chem., 55* (1984) 54.
20 D. Aurbach, M. L. Daroux, P. W. Faguy and E. Yeager, *J. Electrochem. Soc., 134* (1987) 1611.